Scaling Laws in Electrospinning of Polystyrene Solutions

Chi Wang,* Chia-Hung Hsu, and Jian-Hua Lin

Department of Chemical Engineering, National Cheng Kung University, Tainan 701, Taiwan, ROC

Received April 18, 2006; Revised Manuscript Received August 17, 2006

ABSTRACT: By tuning the processing variables and solution properties using four different solvents (dimethylformamide, *o*-dichlorobeneze, tetrahydrofuran, and chloroform), polystyrene (PS) fibers were prepared by the electrospinning process to study the effects of these governing parameters on the morphological changes of the charged cone and jet, as well as the diameter and birefringence of the fibers collected. Both jet diameter (d_j) and fiber diameter (d_f) were scaled with the processing variables, i.e., solution flow-rate (Q), applied voltage (V) and working distance (H), with a power law model. Knowledge of these exponents provided insight into how to manipulate the electrified jet and spun fibers for a given solution. Results showed that Q was the dominant factor in determining the fiber diameter and the Q dependences of d_j and d_f were approximately scaled with: $d_j \sim Q^{0.5}$ and $d_f \sim Q^{0.25}$. The applied electric field (V/H) did affect the cone volume and the length of the electrified jet. Either increasing V or decreasing H produced a slightly thinner jet and smaller fiber, but the effects were not significant due to the limited processing range available for the stable cone-jet mode, and the nonuniformity of the electric field resulting from the point-to-plate electrode configuration used in this study. Regardless of the variations of the processing variables (Q, V, and H), a master curve between d_j and d_f was found for a solution with fixed properties, from which a simple equation was obtained and expressed by: $d_f \sim m d_j^{0.45}$ where m was a prefactor depending upon solution properties, such as the viscosity (η_o), conductivity (κ) and surface tension. Values of m were found to be lower for solutions with lower viscosity and/or higher conductivity, and were successfully scaled to be as follows: $m \sim \eta_o^{0.38}\kappa^{-0.12}$. As far as the solution properties were concerned, the concentration emerged as the most important parameter because of its interaction with all aspects of the electrospinning process. The rheological properties of the polymer solution showed a significant effect on the formation of smooth electrospun fibers. On the basis of the Graessley's concentration-molecular weight diagram, various PS fiber morphologies were discussed and the minimum polymer concentration at a given polymer molecular weight required for preparing smooth PS fibers could be estimated. For the present PS solutions, a scaling law was found between the fiber diameter and solution viscosity: $d_f \sim \eta_o^{0.41}$, if other governing parameters (Q, V, H, κ, and surface tension) were fixed.

1. Introduction

Driven by the wide-spread interest in the nanofiber applications, a considerable amount of research has been aimed at gaining a better understanding of the electrospinning process which is a potential process to prepare polymer fibers with a diameter ranging from micro- to nanometer scale depending on the spinning conditions.[1−3] Although some polymer fibers can be obtained by electrospinning from the melt,[4−6] majority of the fibers are currently prepared from the solution state due to its advantages of low viscosity and controlled conductivity. Three main issues are involved to obtain the desirable fibers, i.e., polymer solution properties, processing variables, and the spinning environments. The properties required for an appropriate solvent for the selected polymer are good miscibility, low boiling point, low surface tension and high conductivity (or dielectric constants).[7−12] In contrast with electrospraying, the prerequisite for the fiber formation is the existence of sufficient entanglement density in the polymer solutions.[13−15] Increasing the solution viscosity (concentration) will prohibit the formation of beaded fibers and increase the fiber diameter. As far as processing variables are concerned, the flow-rate, applied voltages, working distance and capillary diameter are essential to be considered.[16−21] Atmosphere control (humidity and temperature) of the spinning environment is also crucial sometimes to certain polymer solutions which could interact with the moisture.[22,23] By manipulation of all these parameters, a variety of structure differences of the electrospun fibers can be obtained.

Electrospinning is involved with the polymer flow with free surface after emerging from a capillary, followed by the bending and stretching of the jet due to the surface charge repulsion.[24−27] Most of the previous work in the literature has focused on the relation between the processing parameters and fiber morphology, leaving the important subjects of the free surface variations unexplored. To manipulate the free surface of the electrified jet is the first and determinant step to control the morphology of the electrospun fibers. A crucial question is as follows: How do these processing parameters affect the flow free surface, such as the Taylor cone, jet length, and jet diameter? We believe there should be a more intimate relation between the fiber morphology and the cone/jet dimensions, rather than the processing parameters alone. To fulfill this knowledge gap is our main objective of this study. In this article, effects of solution properties and processing variables on the Taylor-cone volume, jet diameter, jet length, bending instability, and the morphology as well as the birefringence of the collected PS fibers were reported. Some general empirical laws relating fibers diameters to processing variables and jet diameters were discussed to give a deep insight into manipulate the fibers desired. In addition, the minimum polymer concentration, at a given PS molecular weight, required for preparing smooth electrospun PS fibers was determined based on our rheological measurements and the Graessley's concentration−molecular weight diagram.

* Corresponding author. Fax: +886-6-2344496. Telephone: +886-6-2757575 Ext 62645. E-mail: chiwang@mail.ncku.edu.tw.

10.1021/ma060866a CCC: $33.50
Published on Web 10/07/2006

Table 1. Properties of Polystyrene and Solvents Used

	δ (cal/cm^3)$^{0.5}$	dielectric constant	κ (μS/cm)	γ (dyn/cm)	ρ (g/cm^3)	T_b (°C)	η_s (cp)
PS	9.1				1.06	-	-
THF	9.1	7.6	9×10^{-2}	26.4	0.889	66	0.46
CF	9.3	4.8	1×10^{-4}	26.5	1.480	61	0.51
o-DCB	10.0	9.9	3×10^{-5}	35.6	1.300	180	1.32
DMF	12.1	36.7	6×10^{-2}	35.2	0.944	153	0.80

2. Experimental Section

2.1. Solution Preparation and Properties. Polystyrenes with four different molecular weight (MW = 4.0K, 100K, 300K, 1880K) weights were used in this study. Major work were conducted using PS with MW = 300K, which was a commercial product by Chi-Mei Co. and had a polydispersity index (M_w/M_n) of 2.3. The other three PS with a low M_w/M_n (~1.2) were purchased from Aldrich Co. Four different solvents, i.e., dimethylformamide (DMF), tetrahydrofuran (THF), chloroform (CF), and *o*-dichlorobenzene (*o*-DCB), were used to prepare PS solutions. The solubility parameter (δ), dielectric constant, conductivity (κ), surface tension (γ), density (ρ) and boiling temperature (T_b) and viscosity (η_s) of the solvents were tabulated in Table 1. On the basis of the solubility parameter difference, it is apparent that CF and THF are good solvents but DMF is a poor solvent for PS. Three various salts were applied to increase the solution conductivity; triethylbenzylammonium chloride (TEBAC) used for the DMF and CF solutions, tetra-*n*-butylammonium perchlorate (TBAPC) for the *o*-DCB solution and lithium perchlorate ($LiClO_4$) for the THF solution. To prepare solutions with different weight percent concentrations, weighted amounts of polymers and solvents were mixed for several hours until homogeneous solutions were obtained. The salt concentration was relative to the mass of the solvent used. Filtration and degassing were occasionally performed to remove the impurity and small bubbles in the solution.

All measurements of solution properties were taken at 25 °C. Surface tension and conductivity of the prepared solutions were measured using Face surface tension meter (CBVP-A3), and Consort conductivity meter (C832), respectively. Linear viscoelastic properties of the solutions were measured in a Rheometrics (ARES) using a cup-and-bob feature. Oscillatory shear mode was used to determine the storage modulus $G'(\omega)$ and loss modulus $G''(\omega)$ over a range of frequencies. Zero shear viscosity η_o was determined from the loss modulus data at low frequencies: $\eta_o = \lim_{\omega \to 0} G''(\omega)/\omega$. Recoverable shear compliance J_s^o was determined from the storage modulus data at low frequencies: $J_s^o = 1/\eta_o^2 \lim_{\omega \to 0} G'(\omega)/\omega^2$. The relaxation time τ_o was estimated by: $\tau_o = \eta_o J_s^o$.[28]

2.2. Processing and Measurements. During electrospinning, the homogeneous PS solution was delivered by a syringe pump (Cole-Parmer) at a controlled flow-rate (Q = 0.03−18 mL/h) through PTFE tubing to the stainless needles (Hamilton, outer diameter = 1.47 mm) where a high electrical voltage (Bertan, 205B) was applied. To construct a point-to-plate electrode configuration, a steel net (30 × 30 cm^2) was used as a collector for the electrospun fibers at a working distance of H below the needle tip. When volatile solvents (such as THF and CF) were used, the Taylor cone was frequently dried out during the process, giving rise to the cone blockage problem. When the DMF solvent was used, on the other hands, the moisture adjacent to the Taylor cone interacted with the PS/DMF solution and a thin layer of PS gel was readily developed, resulting in the unstable ejection of liquid jet from the cone. To rule out these problems, a gas jacket[29] was used to introduce either the saturated solvent vapors (using N_2 as carriers) for the THF and CF solutions to blanket the Taylor cone or simply nitrogen gas to drive away the water vapor around the vicinity of the cone. Although the cone blockage problem could be resolved and a continuous process was readily achieved, the morphology of the collected products was significantly dependent upon the flow-rate of N_2. Two length scales have to be considered, i.e., the length from the jacket end to the terminal liquid jet where the bending instability takes place (jet length, l_J) and the effective distance of the blowing N_2 coming out from the jacket end (l_E). When the bending instability was not interrupted by the carrier gas, i.e., $l_E < l_J$ for low N_2 flow-rate conditions, smooth electrospun fibers were collected. Beaded fibers were initially seen for $l_E \sim l_J$ conditions and a transition to the sphere morphology was evidently observed for $l_E \gg l_J$ conditions, where a too high flow-rate of N_2 gas was applied. Hence, various morphological features, either smooth fibers, beaded fibers or spherical particles, can be obtained by simply manipulating the N_2 flow-rate as pointed out previously.[29] In this study, we applied an appropriate N_2 flow-rate to encapsulate the Taylor cone with the desired atmosphere to ensure a continuous spinning process, simultaneously without interrupting the bending instability, i.e., the $l_E < l_J$ case.

Four CCDs were used to observe the electrospinning process during the experiments at room temperature; CCD1 (Sony XC77) for the shape variation of Taylor-cone at the needle tip, CCD2 (Sony CCDTRV53) for the liquid jet emitting from the Taylor-cone bottom due to the electric repulsion, and CCD3 for the bending instability envelope. CCD3 was a high-speed camera (Redlake, Motion Pro 10000) to capture an image at a frame rate of 10000 frame/s. Laser diffraction was used to monitor the diameter variation of liquid jet from the Taylor-cone bottom to the point where bending instability took place. A 1 mW He−Ne laser with a pinhole of 1 mm diameter was used as light source and the diffraction patterns on a screen were collected by CCD4 (Sony XC77) and further analyzed by the Inspector software. The liquid jet diameters (d) were determined by the first maximum of the diffracted intensity using: $d = 1.43\lambda X/Y$, where λ was the wavelength of the laser light (632.8 nm), X was the distance from the jet to the screen, and Y was the distance between the beam center and the first intensity maximum.[30] The morphology and diameter of the as-spun fibers were observed and measured using a scanning electron microscope (SEM, Hitachi S4100) and the fiber birefringence was determined using a polarized optical microscope (Lica Co., DMLP) equipped with a tilting compensator (Leitz Co.).

In this study, the effects of applied voltage (V), flow-rate (Q), working distance (H), polymer volume fraction (ϕ), and salt addition on the electrospinning process were discussed.

3. Results and Discussion

3.1. Functioning Domains for Stable Cone-Jet Mode. Figure 1a shows a typical relation of the applied voltage vs flow-rate for PS/DMF solutions with various concentrations, where the filled and open symbols denote the V_s and V_{us} respectively, representing the lower- and upper-bound voltage for the cone-jet mode spinning at a given solution flow-rate. Hence, the functioning domains[31,32] defined as the operating ranges of voltages and flow-rates used for electrospinning of the cone-jet mode were determined. It should be noted that the solution viscosity increases with PS concentration (as given in Figure 1a) but the surface tension remains intact regardless the PS content, being similar to pure DMF (35.2 dyn/cm). Since PS chains are nonconducting, the main charge carrier in the PS/DMF solution is the DMF solvent. Thus, the solution conductivity decreases with increasing PS content, from 0.54 μS/cm for the 6 vol % down to 0.20 μS/cm for the 23 vol % solution.

Generally speaking, the voltage required for maintaining cone-jet mode is larger at a higher flow-rate. Depending on the solution properties, however, the functioning domains are different from one another and sometimes rather limited,

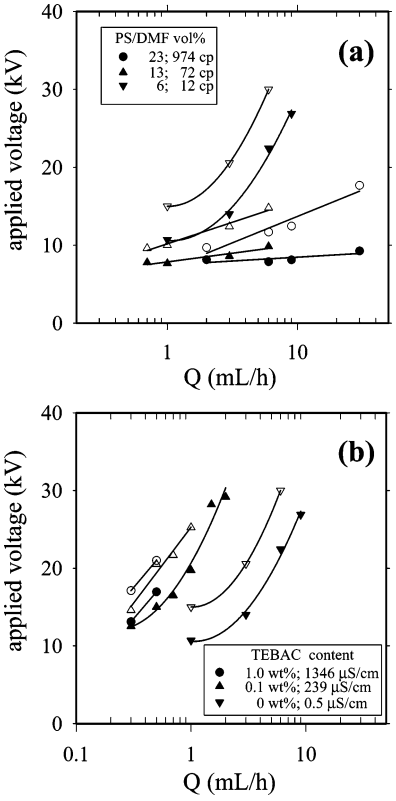

Figure 1. Functioning domains showing the range of operating voltages required for the stable cone-jet spinning mode; filled symbols for the lower bound voltage, V_s, and open symbols for the upper bound voltage, V_{us}: (a) concentration effects, PS/DMF with various PS vol % and the corresponding viscosity is displayed; (b) conductivity effects, 6 vol % PS/DMF with various wt % TEBAC and the corresponding conductivity is shown. H is fixed at 14 cm. Other solution properties in part a are $\gamma = 35.9$ dyn/cm and $\kappa = 0.5$ μS/cm for the 6 vol % solution; $\gamma = 35.9$ dyn/cm and $\kappa = 0.4$ μS/cm for the 13 vol % solution; and $\gamma = 36.7$ dyn/cm and $\kappa = 0.2$ μS/cm for the 23 vol % solution. In part b, the viscosity and surface tension of 6 vol % solutions are unchanged regardless the TEBAC addition (0.1−1.0 wt %).

especially at low flow-rates and high PS contents. At a given Q, both the V_s and the operating voltage range ($V_{us}-V_s$) are lower for the solutions with higher viscosities, indicating that a higher electric field is required for less viscous solutions to develop a stable cone-jet mode. This unexpected phenomenon is attributed to the variation of Taylor cone due to its change of size and shape from concave to convex (as shown in the inset of Figure 2) for solutions with gradually reducing PS contents. A larger convex-shaped cone gives rise to a larger surface area, thereby requiring a higher applied voltage to reach a critical surface charge for issuing a jet from the apex. When Q is too high, the inertial term of flow becomes important, resulting in a continuous jet from the needle tip to the collector in the absence of bending instability. On the other hand, stable cone-jet mode disappears at a sufficiently low Q, plausibly due to the insufficient solution delivered to the controlled cone volume after the jet formation at the apex of the meniscus. In other words, the volume of Taylor cone fluctuates with time during electrospinning and a steady volume is never reached, giving rise to the intermittent jet formation. The minimum Q for stable cone-jet mode was found to depend on the solution viscosity; being 1.0, 0.7, and 2.0 mL/h for 6, 13, and 23 vol % solution, respectively. Hence, a steady electrospinning of 23 vol % PS/DMF solutions is infeasible for Q lower than 2.0 mL/h.

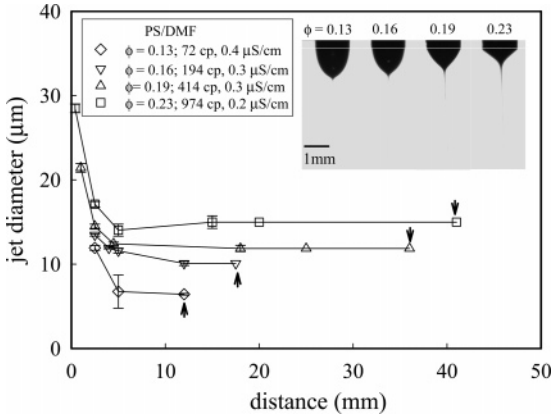

Figure 2. Concentration dependence of the jet diameter as a function of distance from the apex of the Taylor cone. The solution viscosity and conductivity are displayed and the images show the morphologies of the Taylor cone. The solution surface tension remains unchanged at ~36 dyn/cm. $Q = 3$ mL/h, $H = 14$ cm, and 10 kV.

For the 6 vol % PS solution, addition of TEBAC salts leads to an effective increase in the conductivity, being 239 and 1346 μS/cm respectively for 0.1 and 1 wt % TEBAC content, but the viscosity and surface tension of the PS solutions remain unchanged, being 11.9 cP and 35.9 dyn/cm respectively. As shown in Figure 1b, the functioning domain is also varied with the solution conductivity. The higher conductivity the solution is, the larger the applied voltage required to develop a cone-jet mode. On the basis of the observation of cone morphology being discussed in section 3.2, the cone volume increases with increasing solution conductivity, which reduces the surface charge density and in turn a larger V is required to issue a stable jet. As the conductivity increases, moreover, the maximum Q for stable cone-jet mode is reduced and the functioning domain becomes narrower, which is consistent with previous findings in electrospraying to produce monodisperse droplets.[32] For the solution with 1 wt % TEBAC, the operating Q range for stable cone-jet mode is rather limited, being 0.3−0.5 mL/h. At a flow-rate larger than 0.5 mL/h, in contrast, more than two jets are observed and dance around the Taylor cone clockwisely. The formation of the multiple jets is due to the presence of high surface charge density and high mobility of the solutions used. The details of the multiple-jet effect on the electrospun fibers are currently under investigation and will be reported in a future article. In this following report, stable cone-jet mode with a single jet is ensured to ascertain a process with good reproducibility.

Figure 2 shows the variation of jet diameter along the spinning line until the jet end where bending instability takes place, leading to the infeasibility of jet diameter measurements via laser diffraction method. The last point along each profile stands for the jet end, by which the terminal jet diameter (d_j) is determined and its position denotes the jet length. The inset images are the cone morphologies at various PS concentrations. It is noted that the jet diameter decays rapidly within the first 5 mm from the apex of the Taylor cone and reaches a stable d_j beyond. As the concentration increases, the cone region becomes shorter and concave in profile, the diameter of the electrified jet increases, but the membrane diameter collected on the grounded net remains unaffected. Moreover, for a more concentrated solution, a longer electrified jet is observed, which is in agreement with results obtained by Baumagarten.[33] When plotting the logarithm−logarithm plots of d_j (or d_f) vs η_o, a scaling law exists for the present PS/DMF solutions; i.e., $d_j \sim \eta_o^{0.32}$ and $d_f \sim \eta_o^{0.54}$. Although the derived exponent for the

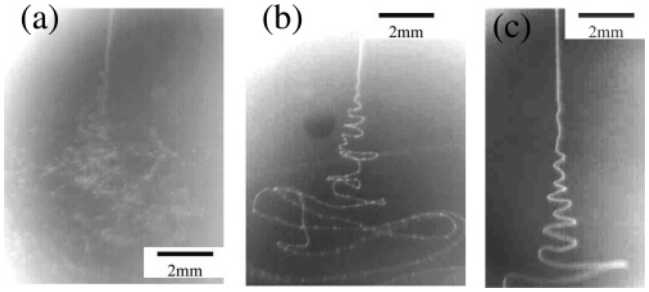

Figure 3. High-speed images of PS/DMF electrospinning jet near the bending instability region (a) $\phi = 0.06$, showing the breakup of liquid jet, (b) $\phi = 0.13$, showing the formation of beaded jets during whipping, and (c) $\phi = 0.23$, showing the presence of smooth liquid jet during whipping. The exposure time was 0.5 ms.

viscosity dependence of d_f is similar to the previously reported value (~0.5) for polyacrylonitrile (PAN)/DMF solutions,[20,33] it is apparently smaller than those for poly(ethylene terephthalate-*co*-ethylene isophthalate)/(CF/DMF) solutions(~0.8),[13] and poly(methyl methacrylate)/DMF solutions (~0.71).[14] However, it should be aware that changing the polymer concentration not only varies the solution viscosity but also may lead to the variations of the conductivity and surface tension.[6,8,10,18] For the present system, solution surface tension is independent of the PS contents. Increasing PS concentration makes the solution viscosity higher but the conductivity lower. Both these effects favor the formation of larger diameters of the electrified jet and as-spun fiber, which might give a misleading exponent. To exclusively reveal the viscosity effect on the d_j and d_f, the conductivity of PS solutions has to be adjusted to be identical. The requirements, i.e., PS solutions with different viscosities but constant surface tension and conductivity, have been successfully fulfilled by suitable salt addition. The viscosity effect on the d_j and d_f will be further discussed in section 3.8.

Two features are worthy noting; the first is the change of cone shape from being convex-like to concave-like as the PS concentration is increased, and the second is that the presence of cone-jet mode is not the prerequisite of the formation of smooth fibers. For the 6 vol % PS solution, as a matter of fact, the presence of cone-jet appearance was readily observed but the jet broke up into charged droplets which traveled toward the electrode under the external electrostatic field's force; a phenomena similar to electrospraying. The first appearance of string with beads on it (beaded fibers) started at the 13 vol % solution and smooth fibers without beads were eventually obtained for the 23 vol % PS solutions. As pointed previously by different groups,[14,15] it indicates that sufficient entanglement numbers are required to electrospin smooth fibers under appropriate conditions, implying the importance of the polymer chain conformations in the solution state (the solution rheology), which will be addressed in the later section. Because of the high-speed motion, conventional camera could not be applied to capture the bending event occurring beneath the jet end.[24−27,33] Accordingly, it was of interest to investigate the imaging of bending instability by high-speed photography, thereby enabling the observation of jet whipping. Figure 3 shows a comparison of high-speed photographs for solutions with 13 and 23 vol % PS contents, possessing a stable cone-jet mode during the same processing conditions as given in Figure 2. Beaded jets are readily discernible for the 13 vol % PS solution in the bending instability region, which leads to the beaded fibers at the collected screen. On the other hand, the 23 vol % PS solution gives rise to smooth jets at the initial stage of the bending instability. Followed by the solvent evaporation during the subsequent bending, smooth PS fibers are produced resulting

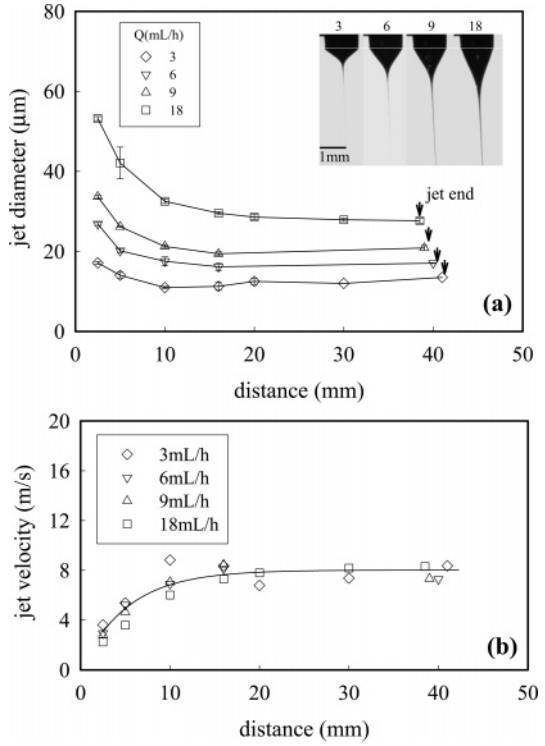

Figure 4. Flow-rate dependence of the profiles of (a) jet diameter, and (b) jet velocity as a function of distance from the apex of the Taylor cone. The images show the morphologies of the Taylor cone (23 vol % PS/DMF solution,$\eta_o = 974$ cP, $\gamma = 36.7$ dyn/cm, $\kappa = 0.2$ μS/cm, $H = 14$ cm, and 10 kV).

from the entanglement enhance due to the concentration increase. On the basis of Figure 3, it seems that there is an intimate relation, either the morphological features or dimension, between the electrified jet end and the correspondingly spun fiber. A relation between the terminal jet diameter and the electrospun-fiber diameter will be explored and presented later. To reveal the processing parameters on the cone/jet/fiber results for a fair comparison, operation conditions for obtaining smooth spun fibers are applied exclusively in the following sections.

3.2. Effects of Solution Flow-Rate (Q) and Conductivity. At a fixed applied voltage and working distance, there exists a processing window for the Q control to form a stable cone-jet electrospinning; a too large Q gives a pulsating mode, but a too small Q results in the inability in the Taylor cone developing. By changing Q, the variation of jet diameter with the distance (z) from the apex of Taylor cone is shown in Figure 4a, where a pronounced decrease is recognized near the apex and the jet diameter quickly reaches an asymptotic value, d_j. The jet diameter profiles are consistent with others[34,35] but a weak z dependence of jet diameter was derived[24,35,36] ($\sim z^{-1/4}$ or $z^{-1/8}$) based on the theoretical considerations for the asymptotic behavior of the jet. As the solution flow-rate is increased, d_j becomes larger, and the jet length is slightly shortened, but the cone height (volume) is apparently increased as shown in the inset images of Figure 4a. Similar trends were also observed for the other PS solutions with different solvents.

The decreasing jet diameter along the jet length might be attributed to two plausible factors; one is the solvent evaporation and the other is the continuous stretching due to the electrical forces, either by the mutual repulsive force on the electrified jet surface or by the electrical fields. As displayed in Figure 4b is the jet velocity profiles by assuming that the solvent evaporation can be neglected and then jet velocity is calculated by: $4Q/\pi d_j^2$. It is interesting to note that the velocity of jet

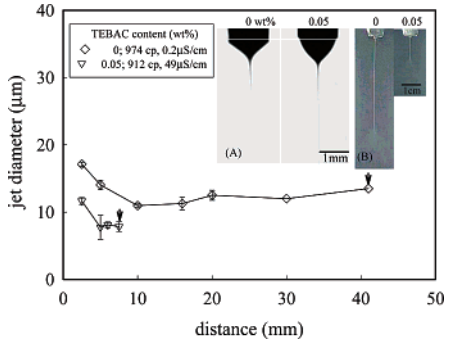

Figure 5. Solution−conductivity dependence of the jet diameter as a function of distance from the apex of the Taylor cone. The solution viscosity and conductivity are displayed and the images show the morphologies of the Taylor cone (A) and the electrified jet (B) (23 vol % PS/DMF solutions, $Q = 3$ mL/h, $H = 14$ cm, and 10 kV).

reaches a plateau value of ca. 8 m/s within first 10 mm traveling length regardless of the Q used. In comparison with the fluid velocity in the needle, ~1 mm/s, it is rather intriguing to note the high acceleration of jet velocity due to the driving force associated with electric repulsions. The traveling time for fluids from the cone apex to the jet end is rather short, ca. 6.7 ms, which further supports the assumption of limited evaporation of DMF solvent in consideration of its high boiling temperature. Hence, the decreasing jet diameter along the jet length is primarily dependent on the electrical forces and the polymer concentration from the cone vertex to the jet end is hardly affected. Moreover, the elongational rate is as high as ~800 s^{-1} when the fluids eject from the cone apex and plug flow patterns are developed near the jet ends, as shown in Figure 4b. Although the terminal jet velocity is independent of the Q, solution viscosity did play a role in determining the jet velocity. According to Figure 2, in fact, the terminal velocity increases with decreasing viscosity and an extremely high jet velocity of 25 m/s can be reached for the 6 vol % PS solution with a viscosity of 10 cP, leading to an elongational rate as high as 1000 s^{-1}.

Because of the viscoelastic characteristics of polymer solutions, viscoelasticity becomes important in cases where the relaxation time (τ_o) of polymer chains is of the same order of magnitude or larger than the time scale of the deformation. The ratio of these two time scales is called the Deborah number,[35] and is expressed as $De = \tau_o/L/v_j \sim \tau_o\dot{\epsilon}$, where $\dot{\epsilon}$ is the elongational strain rate. Depending on PS concentrations, the values of τ_o are in the range of 1−10 ms (as given in Figure 12c), which gives rise to De in a range of 1−10, suggesting that transient effects are important and relaxation phenomena dominates the process. Thus, elasticity plays an important role in the jet adjacent to the cone apex, where significant stretching of the polymer chains is evident[26] due to the convergent flow and a high degree of chain orientation is developing. After the jet velocity is stable, the elongational strain rate becomes small enough that Newtonian-fluid flow is applicable and the inertial term is dominant.

On addition extreme amount of TEBAC salts (0.05 wt %) into the 23 vol % PS/DMF solution, the solution conductivity increased significantly from 0.2 μS/cm to 49 μS/cm but others properties (viscosity and surface tension) remained relatively unchanged. For this more conductive solution, similar trends of the Q dependence of the cone height and jet length were observed, i.e., larger cone volume with shorter jet for increasing Q.[37] At a given Q, however, the enhanced conductivity leads to the cone/jet morphologies having a larger cone and shorter jet, as shown in Figure 5, in comparison with the solution

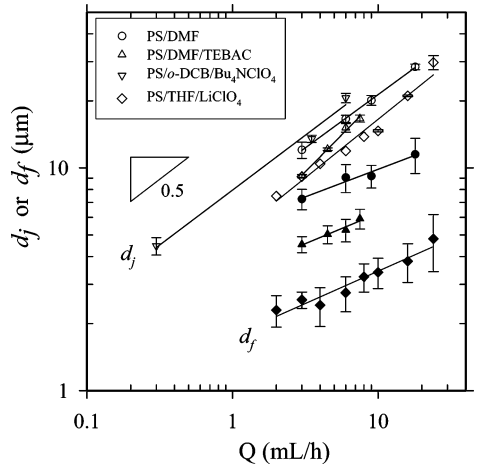

Figure 6. Flow-rate effects on the terminal jet diameter d_j (open symbols) and fiber diameter d_f (filled symbols). $H = 14$ cm, 10 kV, and the Q range available for stable cone-jet mode is studied for the scaling law. Key: (○) 23 vol % PS/DMF, $\eta_o = 974$ cP, $\gamma = 36.7$ dyn/cm, $\kappa = 0.20$ μS/cm; (△) 23 vol % PS/DMF with 0.01 wt % TEBAC, $\eta_o = 907$ cP, $\gamma = 36.7$ dyn/cm, $\kappa = 4.45$ μS/cm; (▽) 17 vol % PS/*o*-DCB with 0.5 wt % Bu_4NClO_4, $\eta_o = 514.2$ cP, $\gamma = 36.6$ dyn/cm, $\kappa = 11.15$ μS/cm; (◇) 18 vol % PS/THF with 0.05 wt % $LiClO_4$, $\eta_o = 291$ cP, $\gamma = 24.2$ dyn/cm, $\kappa = 1.15$ μS/cm.

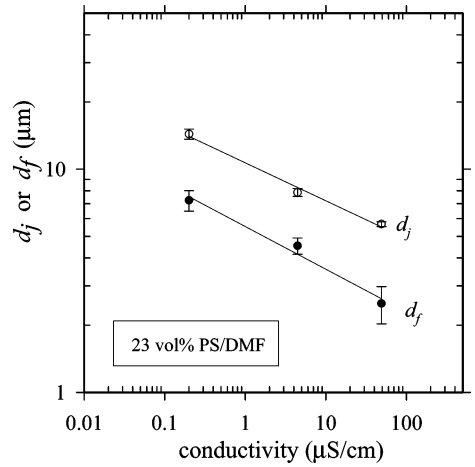

Figure 7. Solution conductivity effects on the terminal jet diameter d_j (open symbols) and fiber diameter d_f (filled symbols) (23 vol % PS/DMF solution with various TEBAC contents; the viscosity is ranging from 907−974 cP and surface tension is unchanged).

without salts. It is of significance to note the reduction of jet diameter to produce a jet velocity as high as ~10 m/s, suggesting a higher elongational strain rate for the more conductive solution.

For four different PS solutions with various properties, Figure 6 shows the Q dependence of the measured d_j (open symbols) and the as-spun fiber diameter, d_f (filled symbols). We found that both d_j and d_f increased with Q and followed a power law model, i.e., $d_j \sim Q^{0.48}$ and $d_f \sim Q^{0.25}$ for the PS/DMF solution, $d_j \sim Q^{0.66}$ and $d_f \sim Q^{0.27}$ for the PS/DMF/TEBAC solution, $d_j \sim Q^{0.44}$ and $d_f \sim Q^{0.23}$ for the PS/THF/$LiClO_4$ solution, $d_j \sim Q^{0.49}$ for the PS/*o*-DCB/Bu_4NClO_4 solution. The exponent for the d_j-Q relation is in accordance with the theoretical considerations: $d_j \sim Q^{1/2}$ derived by Cañán-Calvo,[36] whereas a larger exponent ($d_j \sim Q^{2/3}$) has been proposed by Fridrikh et al.[38] based on a simple assumption of $d_f = \phi^{0.5}d_j$, which may not be valid since different exponents for the Q dependence of the d_j and d_f are obtained experimentally as shown in Figure 6. Experimentally, hence, we found that there is a scaling law between d_j (or d_f) and Q, and the exponent for d_j is ca. two times larger than that for d_f.

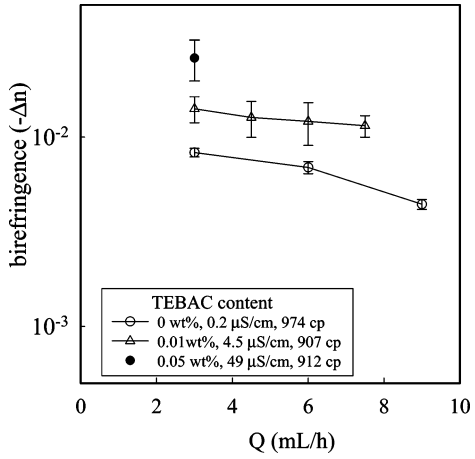

Figure 8. Flow-rate and conductivity effects on the fiber birefringence (23 vol % PS/DMF with various wt % TEBAC, H = 14 cm, 10 kV).

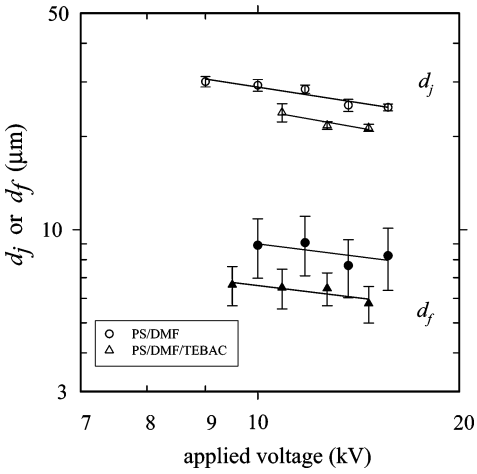

Figure 9. Voltage effects on the terminal jet diameter d_j (open symbols) and fiber diameter d_f (filled symbols). Key: (○) 23 vol % PS/DMF, Q = 18 mL/h, H = 14 cm, voltage limits = 9−13 kV; (△) 23 vol % PS/DMF with 0.01 wt % TEBAC, Q = 8 mL/h, H = 14 cm, voltage limits = 9.5−12.5 kV.

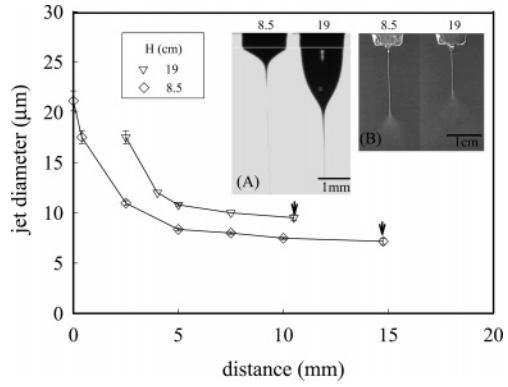

Figure 10. Working-distance dependence of the jet diameter as a function of distance from the apex of the Taylor cone. The images show the morphologies of the Taylor cone (A) and the electrified jet (B) (23 vol % PS/DMF with 0.01 wt % TEBAC, η_o = 907 cP, γ = 36.7 dyn/cm, κ = 4.45 μS/cm, Q = 3 mL/h, 10 kV).

To enhance the solution conductivity, soluble salts are usually added in the polymer solution, which may also change the surface tension and viscosity of the solutions,[11,39] depending on the system. The conductivity dependences of d_j and d_f are shown in Figure 7 where the 23 vol % PS/DMF solutions with various amount of TEBAC were used to give a wide range of solution conductivity but the surface tension and viscosity

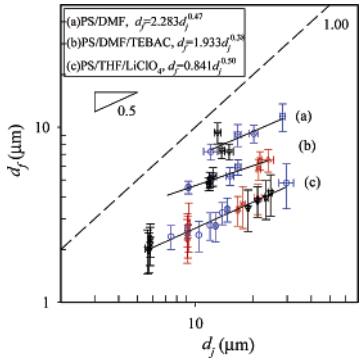

Figure 11. Correlation between fiber diameter (d_f) and jet diameter (d_j) for various solutions electrospun under different conditions. Line a: 23 vol % PS/DMF solution. Line b: 23 vol % PS/DMF with 0.01 wt % TEBAC solution. Line c: 18 vol % PS/THF with 0.05 wt % $LiClO_4$ solution. Key: (○) flow-rate effect; (△) voltage effect; (▽) working distance effect. The processing windows depend on the solution properties. For solution c, for example, the limits available for our scaling law are as follows: Q = 0.8−24 mL/h, H = 9−26 cm, and 9.0−17.5 kV. The dash line gives a slope of 1.0 and the solid lines give the regression results.

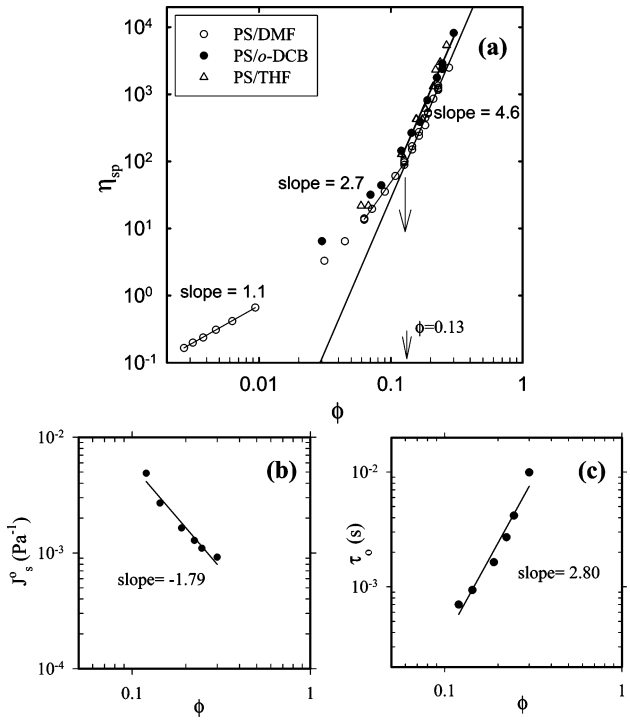

Figure 12. Volume fraction dependence of the (a) specific viscosity for various solutions, (b) recoverable compliance, and (c) relaxation times for PS/*o*-DCB solutions.

remained relatively unchanged.[39] In contrast with Q dependence, a weak scaling exponent is derived: $d_j \sim \kappa^{-0.17}$ and $d_f \sim \kappa^{-0.19}$. The conductivity dependence of jet diameter is in good accordance with the theoretical prediction: $d_j \sim \kappa^{-1/6}$.[36] The low exponent dependence is consistent with previous findings showing that d_f reduction is significant after small amount of salts addition in the less conductive solutions; adding more salt is however unable to effectively produce finer fibers as expected.[9,11,16,39] In other words, sufficient solution conductivity is required to obtain the desirable d_f, but it is Q rather than κ playing a dominant role in consideration of their relative exponents. The scaling law gives us a deep understanding of how to control the terminal jet diameter, and of how we might be able to predict the diameter of electrospun fibers.

CDV

Table 2. Effects of Applied Voltage on the Morphologies of the Electrified Cone and Jet as Well as the Electrospun Fibers

solution	voltage (kV)	cone height (mm)	jet length (mm)	d_j (μm)	d_f (μm)	l_f/l_j (−)	$\Delta n \times 10^2$
PS/THF/	9.0	1.87	13.3	9.24	2.81 ± 0.88	1.95	0.92
$LiClO_4$	9.5	1.11	16.0	9.16	2.64 ± 0.57	2.17	1.03
	10	1.03	17.1	9.14	2.48 ± 0.43	2.44	1.18
	11	0.69	19.9	9.13	2.45 ± 0.66	2.50	1.35
	12	0.40	21.7	9.07	2.32 ± 0.65	2.75	1.59
PS/DMF/	9.5	2.46	6.3		6.64 ± 0.96		1.01
TEBAC	10.5	1.32	7.3	23.9	6.50 ± 0.95	3.11	1.17
	11.5	0.92	7.8	21.7	6.46 ± 0.79	2.60	1.36
	12.5	0.58	8.7	21.3	5.77 ± 0.78	3.13	1.71

[a] Solution properties and operation conditions were as follows: (1) PS/THF/$LiClO_4$ solution, 18 vol %, 0.05 wt % salt, $\kappa = 1.15$ μS/cm, $\eta_o = 291$ cP, $\gamma = 24.2$ dyn/cm, $Q = 3$ mL/h, $H = 14$ cm, and the voltage range for stable cone-jet mode was 9−12 kV; (2) PS/DMF/TEBAC solution, 23 vol %, 0.01 wt % salt, $\kappa = 4.45$ μS/cm, $\eta_o = 907$ cP, $\gamma = 36.7$ dyn/cm, $Q = 8$ mL/h, $H = 14$ cm, and the voltage for stable cone-jet mode was 9.5−12.5 kV.

For the PS/DMF 23 vol % solutions, the diameter of the collected membrane (spinning area) remains constant regardless of the Q used but the fiber birefringence is found to decrease slightly with increasing Q (Figure 8). When the solution conductivity is enhanced by adding the salts, both the membrane diameter and birefringence of the as-spun fibers are increased, indicating the spinning effectiveness associated with the electric repulsive forces. It should be noted that the fiber birefringence obtained by electrospinning is equivalent to that for melt-spun PS fibers at a drawdown ratio[40] of ca. 200. The Herman's orientation factor of the electrospun PS fibers is estimated to be 0.067 by assuming the intrinsic birefringence of PS being −0.15.[41]

3.3. Effects of Applied Voltages (V). Increasing applied voltage at a given H and Q, the cone height (or volume) was gradually reduced but the jet length was increased. Ultimately, the contracted cone interacted with the needle surface at a sufficiently high voltage and interruption of the stable cone-jet spinning mode occurred. The voltage range available for stable cone-jet mode was rather limited; i.e., V_{us}/V_s was generally smaller than 2.0 as shown in Figure 1. Typical results of the voltage effects are displayed in Table 2, showing that the voltages required for the stable cone-jet mode were in the range of 9−12 and 9.5−12.5 kV for the PS/THF/$LiClO_4$ and PS/DMF/TEBAC solutions, respectively. As the applied voltage was increased, both the jet diameter and fiber diameter were slightly reduced but the effect was not pronounced in some systems when their standard deviations were taken into account. In contrast, the fiber birefringence was increased with increasing V, indicating a better chain orientation developed within the electrospun fibers. This finding was not unexpected because one might propose that a larger V should lead to a greater charge density on the jet surface, induce a stronger repulsive force, and result in a smaller d_j. As shown in Figure 9, in fact, PS/DMF solutions show the expected trends and the V dependence of d_j can be scaled as: $d_j \sim V^{-0.57}$, indicating a stronger dependence of d_j on the applied voltage in comparison with the Q effect. For the PS/THF/$LiClO_4$ solution, however, the exponent was negative but very small, ca. −0.04, indicating the insignificant dependence of d_j and d_f on the voltage applied. One should be also aware of the plausible error in determining the power law exponent in consideration of the limited voltage range (9−12 kV, Figure 9) available for the regressions. Nevertheless, similar $d_j - V$ scaling laws with negative sign of approximate exponents have also been obtained in other polymer systems, such as the poly-3-hydroxybutyrtae/CF and PAN/DMF solutions, and the details will be given in a separate article. On the basis of our results, we conclude that the applied voltage shows a negative effect on d_j, which in turn exhibits a similar effect on d_f as shown in Figure 9. Our results are different from the previous findings by Demir et al.[18] and Fennessey et al.[21] on electrospinning polyurethane fibers and PAN fibers, respectively. They reported that jet diameter at a constant distance from the cone apex appeared to increase as the voltage was increased. However, one should be aware that the jet diameter is distance dependence as shown in Figure 4 and the jet length varies with the applied voltage (Table 2), leading to the necessity to determine the precise location of jet end in order to obtain more reliable d_j. In addition, the jet end fluctuates for certain distance owing to the incipient of asymmetric instability.

It is rationalized that significant drawing of jet takes place in the bending instability region, simultaneously resulting in the rapid evaporation of solvent due to the increasing surface area of the whipping jets. Jet drawing becomes infeasible when the jet viscosity increases to a certain level at which the electric repulsive forces is incapable (in vain) to pull the solidified fiber any longer. On the basis of the assumption of volume conservation, we further assumed that the terminal jet with a diameter of d_j was drawn to a specific draw ratio and then the solvent was subsequently evaporated to produce a dry fiber with a diameter of d_f during bending instability Therefore, the draw ratio associated with the bending instability was estimated to be: $l_f/l_j \sim (d_j/d_f)^2\phi$, where l_f and l_j were the phantom lengths of the fiber and jet, respectively and their ratio was termed the drawability of the whipping jet. The larger the drawability of the jet possesses, the higher level of chain orientation is expected. As shown in Table 2, good correlation between the calculated drawability and the fiber birefringence measured is obtained under the condition of voltage changes. Hence, when the PS solutions are electrospun at a higher voltage, thinner PS fibers with larger birefringence are obtained due to the presence of larger repulsive forces in the bending jet which exhibits a stronger drawing (larger l_f/l_j).

3.4. Effects of Working Distance (H). Due to the point-to-plate configuration for our electrospinning setup, nonuniform electric field was expected and the apparent applied electric field was tentatively expressed by the V/H ratio. By varying H at fixed V and Q, the H effect on the cone/jet/fiber dimensions was discussed. For allowing solvent evaporation during jet whipping, H should be sufficiently larger than the jet length, otherwise the liquid jet will touch down the ground collector and/or wet fibers are obtained. A typical plot of the measured jet diameter along the jet length is given in Figure 10, where a 23 vol % PS/DMF solution with 0.01 wt % TEBAC is tested. Increasing the working distance led to a shorter jet and a longer Taylor cone with a profile from being concave to convex. The typical H dependence of the measured cone/jet/fiber dimensions is given in Table 3. Both d_j and d_f were slightly increased (or relatively unchanged in consideration of the standard deviations) although H had been approximately doubled. These findings suggested that it was the applied V rather than the V/H, which played a dominant influence on the jet and fiber diameters during

Table 3. Effects of Working Distance on the Morphologies of the Electrified Cone and Jet as Well as the Electrospun Fibers[a]

solution	H (cm)	cone height (mm)	jet length (mm)	d_j (μm)	d_f (μm)	l_f/l_j (−)	$\Delta n \times 10^2$
PS/THF/	9	0.90	13.6	5.66 ± 0.17	2.02 ± 0.57	1.41	1.75
$LiClO_4$	14	0.95	13.4	5.74 ± 0.10	1.98 ± 0.51	1.51	1.72
	18	1.33	13.1	5.82 ± 0.14	2.15 ± 0.53	1.32	1.38
	21	1.64	12.9	5.85 ± 0.09	2.30 ± 0.50	1.16	1.00
PS/DMF/	10	1.01	9.5	11.69 ± 0.23	4.72 ± 0.40	1.41	1.39
TEBAC	12	1.14	9.3	11.90 ± 0.14	4.74 ± 0.40	1.45	1.36
	14	1.25	9.0	11.88 ± 0.21	5.01 ± 0.52	1.29	1.22
	16.5	1.93	9.0	12.34 ± 0.53	5.24 ± 0.64	1.28	1.20

[a] Solution properties were the same as those given in Table 2 and the operation conditions were as follows: (1) PS/THF/$LiClO_4$ solution, $Q = 0.8$ mL/h, 7.5 kV, and the available H for the stable cone-jet mode was 9−21 cm; (2) PS/DMF/TEBAC solution, $Q = 3$ mL/h, 8.0 kV, and the available H for the stable cone-jet mode was 10−16.5 cm.

electrospinning when point-to-plate electrode configuration was used. As shown in Table 3, however, the jet drawability and fiber birefringence became smaller when H was increased. As expected, the diameter of the nonwoven matt collected was bigger for a larger H. Increasing the conductivity by adding 0.01 wt % TEBAC leads to a similar dependence of working distance on the cone/jet/fiber properties.

3.5. Scaling Law Between d_j and d_f for a Given Solution. As given in Figure 11 are the plots of measured d_j and the corresponding d_f for three PS solutions with various solution properties. The circles correspond to the flow-rate effect alone while keeping other processing variables (V and H) fixed. Similarly, the triangles and inverse triangles denote the effects of changing applied voltage and working distance, respectively. Regardless of the processing variables (Q, V, and H), it is of interest to note the superposition of all measured data for a given solution with fixed properties (viscosity, conductivity, and surface tension), and the diameter of the electrospun fibers can be scaled with the jet-end diameter with an exponent of 0.38 ∼ 0.50 determined from the linear regression. It should be also noted that limited operating windows for each variables are available to obtain stable cone-jet mode which produces reproducible fiber morphologies, as mentioned previously. Among all the three processing variables, V is the most limited one but a relatively wide range of Q (ca. 0.1−10 mL/h) can be readily controlled to produce jets with various diameters. Therefore, controlling the flow-rate is a more effective approach in varying the jet diameter and thus fiber diameter produced. In other words, a thin electrified jet eventually produces small fibers, whose diameter can be estimated with a simple relation:

$$d_f = m(\eta_o, \kappa, \gamma) d_j^{0.45} \quad (1)$$

by taking the average of the exponents, where m is a prefactor related with the solution properties only. As shown in Figure 11, at a given d_j the value of m is smaller for solutions with lower viscosity and/or higher conductivity, which in turn gives thinner fibers collected. On the basis of Figure 7 together with eq 1, a scaling law is further derived ($m \sim \kappa^{-0.12}$) for the conductivity dependence of m. The viscosity dependence of m will be discussed in the section 3.8. Hence, variations of the processing variables merely change the free surface of the electrified cone and jet, producing various d_j. Once d_j is determined, d_f can be predicted by a scaling law with an exponent of ca. 0.45. This exponent is relatively independent of the solvent type (low volatility for DMF and high volatility for THF). In contrast, an exponent of 1.0 is normally assumed in the electrospraying process, in which sinuous deformation is absent and the size of droplets is a result of the capillary breakup of a charged jet.

3.6. Effects of Polymer Concentrations. Solutions with too high concentrations are difficult to yield thin fibers due to the high solution viscosity. On the other hand, too dilute solutions in the absence of chain entanglements will result in the jet breaking into droplets and give rise to the spherical particles instead of fiber structure on the grounded collector. Thus, the spinnability of polymer solution is relevant to its viscoelastic properties. The determination of the critical concentration (ϕ_c) above which chain entanglement incipiently occurs in the solution state is an important task since the first appearance of fiberlike structure (beaded fibers) is seen. However, smooth fibers will only be produced for solutions with a concentration higher than $1.8-2.5\phi_c$,[13,15] where sufficiently high entanglement density is reached. Figure 12a shows the change in solution viscosity with increasing PS volume fraction. At a given ϕ, it's noted that the solution viscosity is higher in a good solvent (THF, *o*-DCB) than in poor solvent (DMF). The dependence of specific viscosity (η_{sp}) on the polymer content is gradually significant from a dilute solution ($\eta_{sp} \sim \phi^{1.1}$), a semidilute solution ($\eta_{sp} \sim \phi^{2.7}$) to a concentrated solution ($\eta_{sp} \sim \phi^{4.6}$). The rapid viscosity increase at ∼13 vol % suggested the existence of chain entanglement occurring around this concentration,[42] which was further supported by the results of elastic compliance as shown in Figure 12b where a simple relation is derived from the slope: $J_s^o \sim \phi^{-1.79}$. For polymers with monodisperse molecular weight, it is well-known that J_s^o is proportional to $\phi^{-1.0}$ for solutions without entanglements, but is proportional to $\phi^{-2.0}$ for solutions with entanglements.[43] Hence, ϕ_c can be alternatively determined by utilizing the ϕ dependence of J_s^o function owing to the evident slope change. Because of the polydispersity of PS used in this study, our derived exponent is slightly different from the theoretical value. The ϕ dependence of relaxation time shows a power relation with an exponent of 2.8 (Figure 12c); the relaxation time increases from 0.7 ms for the 12 vol % solution to 10 ms for the 30 vol % solution. For concentrations lower than 12 vol %, reliable storage modulus (G') cannot be obtained because of the experimental constraints in torque measurements. Since the data for the 12−30 vol % falls on a straight line (Figure 12 b and c), it further indicates that similar chain topography is developed in these solutions, suggestive of the presence of entanglements in the 12 vol % solution. This is in agreement with experimental observations that fiberlike structure is obtained for the solutions with PS concentrations of 13−19 vol %.

Polymer conformations in the solution state are closely related with the concentration and chain length of the polymer used, giving in turn several concentration regimes which can be distinguished. To reveal various regimes of viscoelastic behavior, the concentration−molecular weight diagram proposed by Graessley is frequently used.[44] A typical diagram for the PS/DMF solution is shown in Figure 13, where five regimes are identified. The boundary line between the dilute and semidilute regimes is given by the overlap concentration c^*, which can be

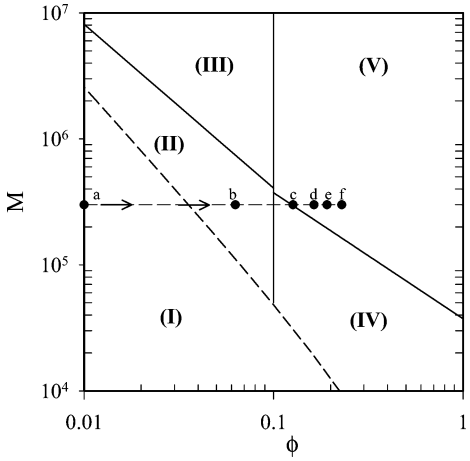

Figure 13. Typical concentration−molecular weight diagram of viscoelastic regimes for PS in DMF solvent. Several regimes for various chain conformations can be identified: (I) dilute, (II) semidilute and not entangled, (III) semidiluted and entangled, (IV) concentrated and not entangled, and (V) concentrated and entangled.

related to the intrinsic viscosity [η] through the equation: $c^* \sim 2.5[\eta]$. For PS, the crossover from the semidulte to concentrated regime occurs for c greater than 0.1 g/cm^3. The viscoelastic properties in the dilute and semidilute solutions ($\phi < 0.1$) are dependent upon the solvent used due to differences in the chain expansion factor, whereas that the molecular weight between entanglements (M_e) is insensitive to solvent power. For sufficiently high polymer concentrations ($\phi > 0.1$), the effect of solvent quality becomes negligible and the scaling of the molecular weight between entanglements with concentration is well established as:$(M_e)_{sol} \sim 18700\phi_c^{-1}$, where 18700 is the M_e in the PS melt. On the other hand, for highly entangled PS in the semidilute regime ($\phi < 0.1$) different scaling rule for the concentration dependence of M_e is derived and expressed to be: $(M_e)_{sol} \sim 10200\phi_c^{-1.3}$.[45] It should be noted that different scaling laws are applied for the concentration dependence of M_e in different regimes. On the basis of the assumption that the critical molecular weight for entanglement M_c is ca. two times of M_e, the boundary between the entangled and nonentangled regimes, i.e., the locus of ϕ_c vs M, was determined and given in Figure 13 (thick solid lines) for monodisperse PS used. Moreover, it should be noted that the transition in Figure 13 is likely to be relatively gradual due to the broad MWD of samples used in this study. Conceptually, electrospinning will be degenerated into electrospraying when the solution characteristics falls in the regimes of I, II, and IV, where chain entanglement is absent. Similar considerations but different expressions have been proposed by McKee et al.[13] and Shenoy et al.[15] in discussing other electrospinning solutions.

The applicability of Figure 13 is found to be rather useful in predicting the electrospun features of PS with a given MW. For examples, the MW of PS that we used is ca. 300K; varying solution concentration from low to high (as shown by the arrows in Figure 13) essentially alters the morphology of the electrospun product from spherical particles (points a and b, 1−6 vol %), beaded fibers (points c−e, 13−19 vol %) finally to smooth fibers (point f, 23 vol %). Our results are in accord with previous findings[13,15] who claimed smooth fibers without any beads are obtained at a concentration higher than $1.75\phi_c$. Hence, Figure 13 provides a convenient guideline to determine the minimum concentration to produce smooth PS fibers at a given PS MW. For examples, a solution with a volume fraction of 0.03 is sufficient for PS with a MW of 1880K to prepare electrospun fibers with fiber structure, a volume fraction higher than 0.37 is required for the PS with a MW of 100K, whereas fiber structure is never observed for the PS with a MW of 4K in all the concentrations prepared.

3.7. Effects of Solvents. It is expected that solvent properties play an important role in determining the spinnability of polymer solutions.[12,46] It seems to us that the solvent possessing high volatility, high conductivity (or dielectric constant) and good solvent characteristic of the polymer is the most desirable one. For all the solvents that we used, the solvent affinity to the PS chains is on the order of THF ~ CF > *o*-DCB > DMF as shown in Table 1, where solubility parameters are given. Moreover, both THF and CF are more volatile than DMF and *o*-DCB. The conductivity of DMF solvent is the highest among them. Although *o*-DCB was a relatively good solvent compared with DMF, no smooth fibers but spherical particles were obtained for PS/*o*-DCB solutions with concentrations even up to 29 vol %, where sufficiently high entanglement density was already reached according to Figure 13. Using the high speed camera, the breakup of electrified jets into droplets of different sizes (similar to Figure 3b) was discernible despite the presence of stable cone-jet mode during electrospinning. The failure to obtain fiber structure was ascribed to the extremely low conductivity (10^{-5} μS/cm) and high boiling temperature of the *o*-DCB solvent. By adding small amount of TEBAC salts, the spinnability of PS/*o*-DCB became feasible and smooth PS fibers were able to prepare under appropriate processing conditions. On the other hand, PS/DMF solutions could be readily electrospun due to the high conductivity characteristics. In comparison with the spinnability of these two solutions, it seems that solution conductivity outweighs the polymer−solvent affinity.

Although the processing time is quite small (~1ms), solvent evaporation might be enhanced when a high volatile solution is delivered from the needle tip to the jet end, where the polymer concentration might be increased. Thus, it is the solution just prior the bending instability, not necessarily the solution in the needle, should possess sufficient entanglement density in order to obtain smooth spun fibers. During the chaotic jet whipping, a significant increase of entanglement density associated with the pronounced solvent evaporation is for certain. Using THF (or CF) as a solvent, PS concentration less than 13 vol % produced merely droplets (diameter ~ 10 ± 2 μm for 6 vol % and 12 ± 2 μm for 12 vol %), 14 vol % solution gave the trace presence of fibers, and finally up to 18 vol % solution generated ribbon-shaped PS fibers having a diameter of 12 ± 6 μm with porous surface. However, the width of PS ribbons was not uniform and "beaded-ribbon" structure was seen, the large knots being 33 μm wide and separated by a distance of ca. 6 μm. Numerous elongated pores (750 nm long and 300 nm wide) along the PS fibers were observed on the surface. The presence of pores is attributed to the interaction of THF (or CF) with moisture during jet whipping, and the pore size is related with the humidity.[21,22] By adding 0.05 wt % $LiClO_4$ salts into 18 vol % PS/THF solutions, the solution conductivity was enhanced, leading to the facts that the jet length was significantly reduced and the as-prepared fibers were smooth and thin (2.5 ± 0.7 μm) with reduced pore diameter (60−100 nm). Similar transitions from beaded to smooth fibers were also reported in the literature.[9,11,16,39] The disappearance of beaded fibers might be attributed to the significant migration of the soluble salts to the jet surface under the strong electric field, which in turn produces a core/shell regime within the electrified jet. Thus, phase separation takes place, giving the presence of "polymer-rich" and "polymer-poor" phases in the core and shell fluids,

Table 4. Effects of Solution Viscosity on the Morphologies of the Electrified Cone and Jet as Well as the Electrospun Fibers[a]

wt (%)	η_o (cp)	cone height (mm)	jet length (mm)	d_j (μm)	d_f (μm)	l_f/l_j (−)	$\Delta n \times 10^2$
20	195	0.74	16.5	8.44 ± 0.14	2.38 ± 0.68	2.20	0.89
21	292	1.03	17.1	9.14 ± 0.07	2.48 ± 0.34	2.50	1.18
24	602	0.87	23.0	9.29 ± 0.08	4.15 ± 1.10	1.06	0.64
25	1068	0.97	22.5	9.31 ± 0.18	3.38 ± 0.91	1.67	0.68
27	1388	0.81	25.5	9.61 ± 0.20	4.90 ± 1.51	0.92	0.45
30	2472	0.85	27.8	10.68 ± 0.44	7.41 ± 1.64	0.55	0.29

[a] PS/THF/$LiClO_4$ solutions were used and their conductivity and surface tension were controlled to be constant at 1.15 μS/cm and 24.2 dyn/cm, respectively. The processing variables were fixed at Q = 3 mL/h, H = 14 cm, and 10 kV.

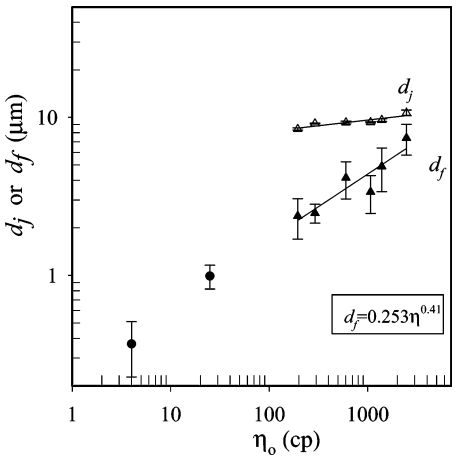

Figure 14. Solution viscosity effects on the terminal jet diameter d_j (open triangles) and fiber diameter d_f (filled triangles) for PS/THF/$LiClO_4$ solutions with various PS (MW = 300K) contents but having a fixed solution conductivity at 1.15 μS/cm by varying $LiClO_4$ salts addition, γ = 24.2 dyn/cm, Q = 3 mL/h, H = 14 cm, and 10 kV, where the viscosity limits available for smooth fiber preparation are 195−2472 cP for PS (MW = 300K). Filled circles are the results of UHMW PS (MW = 1880K).

respectively. Because of this electric-field-induced phase separation, the PS concentration in the core fluid is enriched to prohibit the formation of bead structure. Another plausible cause is the chain conformation change in the PS/THF solution after $LiClO_4$ additions, leading to a lower concentration required for the sufficient chain entanglements.[47]

3.8. Viscosity Dependence of Jet and Fiber Diameters. The surface tension of PS/THF solutions remains constant (~24.2 dyn/cm) regardless of PS and salt concentrations. On the other hand, both solution viscosity and conductivity are dependent upon respective PS and salt concentrations. To exclusively reveal the viscosity effect on the cone/jet/fiber morphologies, we prepared PS/THF solutions with various viscosities (195−2472 cP) by changing PS contents, but a constant conductivity (κ = 1.15 μS/cm) by adding selected amount of $LiClO_4$ salts. Smooth electrospun fibers were ensured from these controlled solutions to exclude the plausible misleading effects induced by the presence of beaded fibers. The results are displayed in Table 4 under the same processing variables (Q, H, and V). As the solution viscosity is increased, the size of the Taylor cone remains relatively unchanged, the electrified jet becomes longer but slightly thicker, and larger fibers with lower birefringence are produced. The calculated jet drawability is significantly small (~0.55) when the solution viscosity is larger than 2000 cP, indicating the infeasibility of "ideal drawing" during jet whipping. Figure 14 shows the η_o dependence of d_j and d_f, from which two simple scaling laws are derived: $d_j \sim \eta_o^{0.07}$and $d_f \sim \eta_o^{0.41}$. Thus, the jet diameter prior to jet whipping is relatively independent of solution viscosity, which is in accord with theoretical consideration.[36] However, the fiber diameter is dominantly controlled by the subsequent jet whipping process; less viscous jets will be stretched more in the bending instability region to produce finer fibers. The derived exponents (0.07 and 0.41) in Figure 14 are significantly different from those (0.32 and 0.54, respectively) obtained previously by Figure 2, in which the solution conductivity was not controlled and beaded fibers were also included for the analysis. Similar deduction may account for the exponent difference in the $d_f-\eta_o$ relation, e.g., 0.80 for the PET copolymer solution[13] and 0.71 for the PMMA solution,[14] reported by other groups due to the coupling effects of viscosity and conductivity (and/or surface tension) variations. Nevertheless, it may also imply that different scaling exponent may apply for polymer solutions with different rheological properties. Using eq 1 together with Table 4, the viscosity dependence of m was derived: $m \sim \eta_o^{0.38}$. In comparison with the conductivity effect, $m \sim \kappa^{-0.12}$, it is evident that solution viscosity shows more promising in controlling the diameter of electrospun fibers.

As shown in Table 4, the minimum viscosity required to prepare smooth PS (M_w = 300K) fibers at room temperature is 195 cP, which produces fibers with a diameter of ~2.4 μm. Compared with other polymers, the difficulty to prepare PS fibers with submicron diameters is attributed to two intrinsic properties possessed by PS chains. The first is the relatively high M_e for chain entanglements in the melt state, which generally leads to a requirement of more concentrated and viscous solutions for fiber electrospinning. The second is its inertness with most of the conductive solvents, leading to the fact that solution conductivity decreases with increasing PS concentrations. At the minimum PS concentrations for electrospinning smooth fibers, the conductivity becomes too low to effectively stretch liquid jets to produce nm sized fibers. To produce nanodiameter PS fibers, two plausible routes are suggested; one is by using ultrahigh MW (UHMW) PS, the other is to carry out a high-temperature electrospinning process. On the basis of Figure 13, a significantly lower concentration is sufficient for electrospinning UHMW PS fibers and the corresponding viscosity is pronouncedly reduced to produce thinner fibers. For example, smooth PS fibers with a diameter of 991 ± 171 and 369 ± 141 nm are successfully electrospun from UHMW PS (MW = 1880K) solutions with a viscosity of 25 and 4 cP, respectively. As shown in Figure 14, it is of importance to note that UHMW PS data (filled circles) fall on the linear regression line of PS results (filled triangles); the superposition is consistent with the previous work by Gupta et al.[14] on electrospinning PMMA solutions with various MWs. In addition, the success in producing submicron PS fibers by high-temperature electrospinning is based on two well-known facts; one is the reduction of solution viscosity at high temperatures, and the other is the temperature independence of the entanglement concentration for a given MW of PS. Temperature effects on the electrospinning process have been studied in this laboratory and the detailed will be presented in another paper.

4. Conclusions

In summary, two main features are required to prepare smooth fibers by electrospinning, i.e., the formation of cone-jet spinning mode and the existence of chain entanglement in the solution at the electrified jet end prior to the bending instability. We have measured the rheological properties of PS solutions with various compositions to reveal the minimum concentration for the chain entanglements and discussed their influences on the electrospun fibers. Moreover, the applicability of the molecular weight-concentration diagram as proposed by Graessley is also provided to guide the process and good agreement with experimental observations is reached. The solution conductivity also plays a key role in determining the fiber spinnability. For the solution possessing insufficient entanglement density for preparing smooth fibers, increasing the conductivity by adding salts will lead to the transformation of fiber morphology from beaded fibers (without salt addition) to smooth fibers at the same polymer concentration.

The processing parameters applied for the electrospinning can be classified into two groups; the first is the solution properties (viscosity, conductivity and surface tension) and the second is the processing variables (flow-rate, applied voltage, and working distance). Variations of the processing variables result in the change of the free surface of the cone-jet which in turn changes the jet diameter, producing electrospun fibers with different diameter and birefringence. Regardless of the processing variables, a master curve between d_j and d_f is obtained for a given PS solution, and a simple relation is derived: $d_f = md_j^n$, where m is a prefactor depending upon the solution properties and the exponent n is approximately constant, $\sim$0.45. As far as the solution properties are concerned, solution viscosity is the most important factor in determining the fiber diameter and a power law relation is derived: $d_f \sim \eta_o^{0.41}$ when the solution conductivity and surface tension are fixed. These simple scaling laws are helpful in guiding the preparation of electrospun fibers desired.

Acknowledgment. The authors are grateful to the National Science Council of Taiwan (ROC) for the research grant (NSC92-2216-E-006-016) that supported this work.

References and Notes

(1) Huang, Z.-M.; Zhang, Y.-Z.; Kotaki, M.; Ramakrishna, S. *Compos. Sci. Technol.* **2003**, *63*, 2223.
(2) Li, D.; Xia, Y. *Adv. Mater.* **2004**, *16*, 1151.
(3) Reneker, D. H.; Fong, H. *Polymeric nanofibers*; ACS Symposium Series 918; American Chemical Society: Washington, DC, 2006.
(4) Larrondo, L.; Manley, R. St. J. *J. Polym. Sci., Part B: Polym. Phys.* **1981**, *9*, 909.
(5) Kim, J. S.; Lee, D. S. *Polymer* J **2000**, *32*, 616.
(6) Lyons, J.; Li, C.; Ko, F. *Polymer* **2004**, *45*, 7597.
(7) Fong, H.; Chun, I.; Reneker, D. H. *Polymer* **1999**, *40*, 4585.
(8) Son, W. K.; Youk, J. H.; Lee, T. S.; Park, W. H. *Polymer* **2004**, *45*, 2959.
(9) Kim, S. J.; Lee, C. K.; Kim, S. I. *J. Appl. Polym. Sci.* **2005**, *96*, 1388.
(10) Lee, K. H.; Kim, H. Y.; Bang, H. J.; Jung, Y. H.; Lee, S. G. *Polymer* **2003**, *44*, 4029.
(11) Lin, T.; Wang, H.; Wang, H.; Wang, X. *Nanotechnology* **2004**, *15*, 1375.
(12) Wannatong, L.; Sirivat, A.; Supaphol, P. *Polym. Int.* **2004**, *53*, 1851.
(13) Mckee, M. G.; Wilkes, G. L.; Colby, R. H.; Long, T. E. *Macromolecules* **2004**, *37*, 1760.
(14) Gupta, P.; G.; Elkins, C.; Long, T. E.; Wilkes, G. L. *Polymer* **2005**, *46*, 4799.
(15) Shenoy, S. L.; Bates, W. D.; Frisch, H. L.; Wnek, G. E. *Polymer* **2005**, *46*, 3372.
(16) Zong, X.; Kim, K.; Fang, D.; Ran, S.; Hsiao, B. S.; Chu, B. *Polymer* **2002**, *43*, 4403.
(17) Zuo, W.; Zhu, M.; Yang, W.; Yu, H.; Chen, Y.; Zhang, Y. *Polym. Eng. Sci.* **2005**, *45*, 704.
(18) Demir, M. M.; Yilgor, I.; Yilgor, E.; Erman, B. *Polymer* **2002**, *43*, 3303.
(19) Deitzel, J. M.; Kleinmeyer, J.; Harris, D.; Tan, N. C. B. *Polymer* **2001**, *42*, 261.
(20) Buchko, C. J.; Chen, L. C.; Shen, Y.; Martin, D. C. *Polymer* **1999**, *40*, 7397.
(21) Fennessey, S. F.; Farris, R. J. *Polymer* **2004**, *45*, 4217.
(22) Megeleski, S.; Stephens, J. S.; Chase, D. B.; Rabolt, J. F. *Macromolecules* **2002**, *35*, 8456.
(23) Casper. C. L.; Stephens, J. S.; Tassi, N. G.; Chase, D. B.; Rabolt, J. F. *Macromolecules* **2004**, *37*, 573.
(24) Hohman, M. M.; Shin, M.; Rutledge, G.; Brenner, M. P. *Phys. Fluids* **2001**, *13*, 2221.
(25) Shin, Y. M.; Hohman, M. M.; Brenner, M. P.; Rutledge, G. C. *Polymer* **2001**, *42*, 9955.
(26) Reneker, D. H.; Yarin, A. L.; Fong, H.; Koombhongse, S. *J. Appl. Phys.* **2000**, *87*, 4531.
(27) Yarin, A. L.; Koombhongse, S.; Reneker, D. H. *J. Appl. Phys.* **2001**, *89*, 3018.
(28) Graessley, W. W. *Viscoelastic and flow in polymeric fluids* in *Physical properties of polymers*, 3rd ed.; Cambridge, U.K., 2004.
(29) Lasrson, G.; Spretz, R.; Velarde-Ortiz, R. *Adv. Mater.* **2004**, *16*, 166.
(30) Khodier, S. A. *Opt. Laser Technol.* **2004**, *36*, 63.
(31) Clopeau, M.; Prunet-Foch, B. *J. Electrostactics* **1989**, *22*, 135.
(32) Chen, D. R.; Pui, D. Y. H.; Kaufman, S. L. *J. Aerosol Sci.* **1995**, *26*, 963.
(33) Baumgarten, P. K. *J. Colloid Interface Sci.* **1971**, *36*, 71.
(34) Spivak, A. F.; Dzenis, Y. A.; Reneker, D. H. *Mech. Res. Commun.* **2000**, *27*, 37.
(35) Feng, J. J. *J. Non-Newtonian Fluid Mech.* **2003**, *116*, 55.
(36) Gañán-Calvo, A. M. *Phys. Rev. Lett.* **1997**, *79*, 217.
(37) Lin, J. H. Preparation of polystyrene-fiber membranes via electrospinning. Master's thesis, National Cheng Kung University of Chemical Engineering, 2004.
(38) Fridrikh, S. V.; Yu, J. H.; Brenner, M. P.; Rutledge, G. C. *Phys. Rev. Lett.* **2003**, *90*, 144502.
(39) Choi, J. S.; Lee, S. W.; Jeong, L.; Bae, S. H.; Min, B. C.; Youk, J. H.; Park, W. H. *Int. J. Biol. Macromol.* **2004**, *34*, 249.
(40) Kang, H. J.; White, J. L. *Intern. Polym. Processing* **1986**, *1*, 12.
(41) Stein, R. S. *J. Polym. Sci.* **1969**, *7*, 1021.
(42) Colby, R. H.; Fetters, L. J.; Funk, W. G.; Graessley, W. W. *Macromolecules* **1991**, *24*, 3873.
(43) Sakai, M.; Fujimoto, T.; Nagasawa, M. *Macromolecules* **1972**, *5*, 786.
(44) Graessley, W. W. *Polymer* **1980**, *21*, 258.
(45) Inoue, T.; Yamashita, Y.; Osaki, K. *Macromolecules* **2002**, *35*, 9169.
(46) Shenoy, S. L.; Bates, W. D.; Wnek, G. *Polymer* **2005**, *46*, 8990.
(47) Rodd, A. B.; Dunstan, D. E.; Boger, D. V. *Carbohydr. Polym.* **2000**, *42*, 159.

MA060866A